THE ASTROPHYSICAL JOURNAL, 393:437–449, 1992 July 10

COHERENT STRUCTURES IN THE UNIVERSE AND THE ADHESION MODEL

LEV KOFMAN[1]
Canadian Institute for Theoretical Astrophysics, University of Toronto, 60 St. George Street, Toronto, Canada M5S 1A1
DMITRI POGOSYAN
Institute for Astrophysics and Atmospheric Physics, Estonian Academy of Sciences, Tartu, Estonia 202444
AND
SERGEI F. SHANDARIN AND ADRIAN L. MELOTT
Department of Physics and Astronomy, University of Kansas, Lawrence, KS 66045
Received 1991 August 23; accepted 1992 January 21

ABSTRACT

We use the adhesion model to study the formation process of large-scale structures due to nonlinear gravitational growth of small initial fluctuations in the universe dominated by dark matter. First, we test the adhesion model against two-dimensional (512 × 512) N-body simulations with initial power-law spectral indices $n = -2, 0, +2$, and various cutoffs. We find that the adhesion model imitates the skeleton of the structure extremely well for all choices for the parameters of the initial spectra until the stage when the nonlinear scale reaches the correlation length R_φ of the initial gravitational potential. The adhesion model naturally explains the origin of large-scale coherent structures such as superpancakes and superfilaments, as a result of coherent motion of clumps due to large-scale inhomogeneities in the initial gravitational potential. This can happen in all kinds of initial conditions, not just traditional "pancake" models. Coherent structures can form up to size $\sim R_\varphi$, and beyond R_φ nonlinear evolution does not produce extended coherent objects. We find that clumps of mass identified in the N-body simulations correspond to several knots in the adhesion model, which influences the way of calculating the mass distribution function. We also find that the distribution functions of velocities and masses of clumps and areas of cells in the adhesion model satisfy self-similar scaling laws of the $n = 2$ model.

Subject headings: dark matter — large-scale structure of the universe — videotapes
Accompanying videotape: ApJ, 393, Part 1, No. 2, Videotape, Segment 1

1. INTRODUCTION

We discuss the formation of the large-scale structure (LSS) in the universe, assuming a global structure of the matter distribution consisting primarily of clusters and superclusters of galaxies with giant voids between them. It is generally accepted that in the present universe most mass exists in the form of dark (nonluminous) matter. At the epoch of the LSS formation under consideration dark matter acts as collisionless dustlike particles without pressure and is governed by Newtonian gravitation only, assuming that the baryon fraction is negligible and that radiative and gasdynamics effects are short-range. In our approach, the LSS is assumed to form from the growth of small primordial inhomogeneities by gravitational instability. The universe is assumed to be flat ($\Omega = 1$), in agreement with the theory of cosmic inflation. Galaxies are idealized as structureless points, and the observed structure luminous matter is assumed to be a tracer of the dark matter distribution. These assumptions are not absolutely necessary. Nevertheless, they are minimal and enough to explain qualitatively how LSS arises. The mathematical problem is reduced to solving a well-known basic nonlinear system (with an evident generalization in multistream flow regions) comprising the continuity equation (Peebles 1980; Zel'dovich & Novikov 1983),

$$\frac{\partial \rho}{\partial t} + 3H\rho + \frac{1}{a}\nabla \cdot (\rho \boldsymbol{v}) = 0 , \tag{1}$$

the Euler equation,

$$\frac{d\boldsymbol{v}}{dt} + H\boldsymbol{v} = -\frac{1}{a}\nabla\varphi , \tag{2}$$

and the Poisson equation,

$$\nabla^2\varphi = 4\pi G a^2(\rho - \bar{\rho}) , \tag{3}$$

where ρ, $\boldsymbol{v}$, φ are the density, peculiar velocity, and peculiar gravitational potential of dustlike matter in the expanding uniform background, which has scale factor $a(t) = t^{2/3}$ and mean density $\bar{\rho} \propto a^{-3}$. For simplicity we assume zero cosmological constant. The initial conditions are defined by the growing model of potential perturbations, for which the linear solution is given by

$$\frac{\delta\rho(\boldsymbol{x}, t)}{\rho} = Aa(t)\nabla^2\varphi , \tag{4}$$

where $A = (\frac{3}{2}H^2a^3)^{-1} = \text{constant}$ for the flat dustlike dark matter–dominated universe. The spatial form of initial inhomogeneities is defined by the initial peculiar gravitational potential $\varphi(\boldsymbol{x})$. Its main properties are as follows: $\varphi(\boldsymbol{x})$ does not change during the linear stage, and its random field contains all information about the particular cosmological model through both the initial spectrum of perturbations and the transfer function, which depends on the type of dark matter.

A quantitative and convincing explanation of the origin of the LSS is still a challenge for theorists. This includes several components: formulation of a theory, developing methods for following the evolution of initial conditions into nonlinear

[1] On leave of absence from Institute of Astrophysics and Atmospheric Physics, Tartu, Estonia 202444.

structures, comparison with observations, etc. In theories based on gravitational instability one of the major goals is to find a solution of the system of equations (1)–(3) in terms of the spatial mass distribution. Since most matter is condensed into gravitationally bound objects at the nonlinear stage, the problem is: Which type of objects have more density contrast and dominate during different epochs of evolution? One has to keep separately in mind the various types of nonlinear objects: spherical virialized clumps, asymmetric pancakes (sheets), and filaments. Voids, of course, are also assumed. The next problem is to find the mass and velocity multiplicity function of such objects.

It is important to clarify that in this paper we are not trying to compare specific models with data, but rather to develop the theory of how small-amplitude fluctuations develop into nonlinear structure. We now have various theoretical approaches to nonlinear gravitational clustering which elucidate different features of the problem. Let us examine each.

Direct extrapolation of linear growth of density field peaks creates a picture in which structure evolves hierarchically (see, e.g., Peebles 1980). Here the smallest mass scales collapse first, forming roughly spherical objects, and they then merge to form similar objects on larger scales. According to the Press-Schechter prescription (Press & Schechter 1974), regions which are initially overdense by a fraction $\delta \equiv \delta\rho/\rho$ locally reverse the background cosmological expansion and form bounded virialized objects. This happens after the universe has expanded by a factor $a = \delta/\delta_c$, where the phenomenological critical level is $\delta_c \sim 1$. To obtain the mass distribution function of the objects, one should smooth the primeval density field with a filter (e.g., Gaussian) of width R_f corresponding to the nonlinear scale $M \sim \bar{\rho} R_f^3$. The Press-Schechter method is based on the variance of the density field smoothed with a window function, $W_k^2(R_\varphi) \propto \exp(-k^2 R_f^2)$ for the Fourier components of Gaussian filtering. This model gives a multiplicity function $f(M)$ for the fraction of mass in objects within mass range $(M, M + dM)$ which is in good agreement with results of N-body simulations (Efstathiou et al. 1988), except for very steep spectra (Williams et al. 1991). Variants of the Press-Schechter method have been applied to the cold dark matter (CDM) model, in which LSS formation has strong features of hierarchical clustering. Treating clusters of galaxies as biased smoothed fluctuations (Kaiser 1984) and the more general treatment of biasing in cosmology (Bardeen et al. 1986) are closely related ideas. For recent developments see Peacock & Heavens (1990) and Bond et al. (1991). Unfortunately, the hierarchical prescription does not give us the location and dynamics of the LSS for cosmologically interesting initial spectra, since usually this type of theory does not study the displacement of mass.

Another powerful model is the Zel'dovich solution (Zel'dovich 1970), which approximately describes the displacement of particles from the unperturbed Lagrangian position $\boldsymbol{q}$ to the Eulerian (comoving) position $\boldsymbol{x}$,

$$\boldsymbol{x}(t, \boldsymbol{q}) = \boldsymbol{q} + a(t)\nabla\Phi_0(\boldsymbol{q}) , \tag{5}$$

due to initial potential perturbations specified by the random field of the velocity potential Φ_0, which is related to the peculiar gravitational potential φ_0 by

$$\varphi_0 = -A^{-1}\Phi_0 ,$$

where A is the constant in equation (4). The spatial structure of the nonlinear density field in the Zel'dovich approximation is defined by the inverse of the determinant of the deformation tensor $\delta_{ij} + a\,\partial^2\Phi_0/\partial q_i\,\partial q_j$. At the moment a_c, in the vicinity of point $\boldsymbol{q}_c$, where the leading eigenvalue of the deformation tensor is $\lambda_1(\boldsymbol{q}_c) = 1/a_c$, the density formally reaches infinity, and the first nonlinear object— a very asymmetric pancake— arises. The Zel'dovich approximation works quite well in the quasi-linear stage until pancake formation (Shandarin, Doroshkevich, & Zel'dovich 1983). In the hot dark matter (HDM) model the pancakes are of the size of superclusters, because of the spectral cutoff of these scales. Ten years ago the success of this theory of LSS was based on pancakes. One might think that pancakes enlarge and form a connected network of sheets and filaments, which exists as an intermediate asymptotic and then decays into isolated, randomly distributed clumps. We will present evidence that for various initial spectra the clumps move coherently into new structures, and that this motion can also be regarded as pancake formation.

Actually, in the basic equations (1)–(3) no intrinsic scale is present. In every model (assuming that the medium is dustlike and φ_0 is nonfractal) the first nonlinear objects are very asymmetric pancakes, and the formation of structure begins with them. A sharp spectral cutoff is *not* required. From equation (5) we can write

$$\nabla_q\left[\frac{(\boldsymbol{x} - \boldsymbol{q})^2}{2a} + \text{const}\right] = A\nabla_q\varphi_0(\boldsymbol{q}) , \tag{6}$$

since $\varphi_0 = -A^{-1}\Phi_0$. This equation inspires a nice geometrical interpretation of the Zel'dovich solution; one can find the Eulerian coordinate $\boldsymbol{x}$ of the particle with initial Lagrangian coordinate $\boldsymbol{q}$ at the chosen time simply by projecting the apex of the paraboloid

$$P = \frac{(\boldsymbol{x} - \boldsymbol{q})^2}{2a} + \text{const} \tag{7}$$

implied by equation (6). Condition (7) is for the osculation of P tangent to the hypersurface $\varphi_0(\boldsymbol{q})$ at point $\boldsymbol{q}$ by adjusting the free constant under the condition that P does not cross φ_0 at any point (Fig. 1 of Kofman, Pogosyan, & Shandarin 1990). Any initial nonfractal gravitational potential, according to equation (7), leads to singularities—caustics. Pancakes inevitably arise in the CDM model, but they can form very early and have cosmologically negligible size. The direct application of the Zel'dovich approximation becomes invalid soon after the formation of the pancakes, so it has been widely believed that the advantages of the pancake scenario do not extend to models like the CDM.

The hierarchical clustering and the pancaking models seem, at first glance, to be competing, and probably even mutually incompatible. However, the metamorphosis which has taken place with pancakes in the adhesion model provides compatibility with both scenarios.

The adhesion model is the next step toward understanding of the nonlinear regime (Gurbatov, Saichev, & Shandarin 1985, 1989; Kofman & Shandarin 1988; Shandarin 1988; Shandarin & Zel'dovich 1989). Numerical experiments show that the thickness of pancakes is considerably smaller than their sizes and the distances between them (Doroshkevich et al. 1980; Dekel 1983; Melott 1983). The idealization is therefore assumed that particles stick together inside pancakes, which become infinitely thin. Adhesion can be mimicked by the artificial viscosity term in the oversimplified equation of motion used in the Zel'dovich solution. That leads to Burgers's equa-

tion (Burgers 1974), admitting an analytical solution. This model based on Burgers's equation with negligible (but *nonzero*!) viscosity deals with the skeleton of the structure, which at an arbitrary time is found directly without intermediate steps by means of the geometrical construction (6) beyond the Zel'dovich approximation. This includes (but is not limited to) the pancakes found in the HDM model. The skeleton of LSS in the model resembles the random packed cellular structure consisting of sheets (pancakes), filaments, and knots. The dynamics of the cellular structure looks like the growth of some cells and shrinking of others, and meanwhile knots merge to form knots of larger mass, corresponding to the hierarchical clustering of knots. Thus, the model includes both hierarchical clustering of the knots and their motion, which under certain conditions looks like pancaking. Kofman et al. (1990), Weinberg & Gunn (1989, 1990), and Nusser & Dekel (1990) demonstrate the ability of the adhesion model to reproduce the results of N-body simulations. However, the analytical calculations of the statistics of matter distribution and motion (Gurbatov et al. 1985, 1989; Doroshkevich & Kotok 1990) were made under the oversimplified assumption of uncorrelated peaks of gravitational potential, as well as identifying a single knot of the cellular structure with the matter clump. The range of applicability of the model (in terms of initial spectra and stages) was not studied.

In this paper we discuss the following questions:

1. The restrictions of the applicability of the adhesion model in terms of the initial conditions.
2. The explanation of the large-scale coherent structures observed in N-body simulations and observational data, on the basis of the adhesion model.
3. A qualitative unification of the pancake and hierarchical clustering models, using the adhesion model.

In § 2 we test the adhesion model by comparing it with direct two-dimensional high-resolution N-body simulations. We make the comparison for pure power-law initial spectra with several indices, $n = -2, 0, +2$, and cutoffs, $k_c = 4, 32, 256$ ($k = 1$ corresponds to the fundamental mode and $k = 256$ to the Nyquist frequency in this case), at various stages [until $(\delta\rho/\rho)_{\text{lin.theor.}} \approx 4000$ in the most extreme case].

To combine hierarchical clustering and pancaking, we need a new qualitative concept reflecting the development of structure. We base this on large-scale deformation of the developed cellular structure due to long-wave perturbations of the peculiar gravitational potential. We show (§ 3) why knots tend to form large-scale coherent structures as a result of large-scale coherent motion of matter. These large-scale, asymmetric, coherent structures made of smaller clumps we call "superpancakes" and "superfilaments," as structures of the next generations. This is in contrast to pancakes and filaments, which form from a continuous medium and are bounded by caustics.

Superpancakes are the main issue of this paper. We demonstrate that the visual alignment of clumps in N-body simulations corresponds to proper pancakes, whose positions can be derived by the geometrical technique of inserting a paraboloid in the smoothed initial gravitational potential. The matter distribution in clumps in N-body simulations (Melott & Shandarin 1990) has been shown to be strongly correlated with pancakes on the scale of nonlinearity of the field by explicitly measuring the cross-correlation amplitude (Beacom et al. 1991, hereafter BDMPS), in agreement with our geometrical result. We urge the reader to examine the accompanying videotape (ApJ, 393, Part 1, No. 2, Videotape, Segment 1) to see the process of formation of superpancakes in various models.

The pancaking continues until approximately the epoch t_φ, when the sizes of structures (the scale of nonlinearity) reach the typical correlation scale of the initial gravitational potential, which we denote R_φ (we formally define and discuss it in § 3). This simple picture leads to an important conclusion: in every cosmological model, including those where structure evolves hierarchically coherent structures can be constructed until the epoch t_φ. Their position is reproduced by inserting paraboloids in the smoothed field of gravitational potential. The intensity of superpancaking is governed by the amplitude of large-scale metric perturbations, while small-scale details are dynamically forgotten. It is important that the superpancaking (coherent motion of clumps) can be observed even until t_φ, as deformation of density contours toward superpancakes. That could be detected, for instance, by the percolation test (Dominik & Shandarin 1992) or in the probability distribution function of smoothed density field (Kofman 1991). It is interesting in connection with the observations demonstrating the existence of large-scale coherent structures like anisotropic superclusters (Oort 1983) and filaments (Giovanelli & Haynes 1982; Chincarini, Rood, & Thompson 1981; Tago, Einasto, & Saar 1986). Especially notable here is the recent discovery of the Great Wall (Geller & Huchra 1989).

Finally, in § 4 we discuss the equation of the mass of bound objects, estimating the volume (area) of the corresponding Lagrangian regions. We show that the clumps of mass identified in N-body simulations correspond to several knots in the adhesion model. This fact, together with the restrictions on applicability obtained in § 2, can significantly change the way of making analytical calculations of the mass distribution function in the adhesion model.

2. THE COMPARISON OF THE ADHESION MODEL WITH N-BODY SIMULATIONS

We now briefly describe the adhesion model, present the numerical code for this model, and compare adhesion calculations to the results of direct N-body simulations for the same initial conditions. Let us use a new time variable $a(t)$ instead of t, and introduce a comoving velocity $\boldsymbol{u} = d\boldsymbol{x}/da = \boldsymbol{v}/a\dot{a}$. Then equation (2) has the form (Kofman 1991)

$$\frac{\partial \boldsymbol{u}}{\partial a} + (\boldsymbol{u}\cdot\nabla)\boldsymbol{u} = -\frac{3}{2a}(\boldsymbol{u} + A\nabla\varphi)\,. \tag{8}$$

In the Lagrangian approach, the right-hand side has the meaning of a force acting on the particle. In a Zel'dovich approximation it is set to zero, corresponding to the free streaming of particles in comoving coordinates. To go beyond the Zel'dovich solution, a viscosity term is added to mimic the gravitational adhesion,

$$\frac{\partial \boldsymbol{u}}{\partial a} + (\boldsymbol{u}\cdot\nabla)\boldsymbol{u} = \nu\nabla^2\boldsymbol{u}\,. \tag{9}$$

We consider the case when the viscosity coefficient $\nu \to 0$ (but $\nu \neq 0$!), so that the viscosity term does not affect the motion of the matter outside the mass concentrations but is very important inside.

Equation (9) is the well-known Burgers equation (Burgers 1974). For the potential problem under consideration it has an

exact analytical solution, which in the limit of $\nu \to 0$ reads as

$$\boldsymbol{u}(\boldsymbol{x}, t) = \sum_\alpha \left(\frac{\boldsymbol{x} - \boldsymbol{q}_\alpha}{a}\right) j_\alpha \exp\left(-\frac{S_\alpha}{2\nu}\right) \Big/ \sum_\alpha j_\alpha \exp\left(-\frac{S_\alpha}{2\nu}\right), \quad (10)$$

where $\boldsymbol{q}_\alpha$ are the Lagrangian points which minimize the action

$$S_\alpha \equiv S(\boldsymbol{x}, a; \boldsymbol{q}_\alpha) = \Phi_0(\boldsymbol{q}_\alpha) + \frac{(\boldsymbol{x} - \boldsymbol{q}_\alpha)^2}{2a} = \min , \quad (11)$$

$$j_\alpha = \left[\det\left(\delta_{ij} + \frac{\partial^2 \Phi_0}{\partial q_i \partial q_j}\right)\right]^{-1/2}\Bigg|_{\boldsymbol{q} = \boldsymbol{q}_\alpha}, \quad (12)$$

considered as a function of $\boldsymbol{q}$ for fixed $\boldsymbol{x}$. Physically, minimizing S means that at the moment $a(t)$ the particle $\boldsymbol{q}_\alpha$ is at the Eulerian point $\boldsymbol{x}$. The minimizing points $\boldsymbol{q}_\alpha$ are those that satisfy the Zel'dovich solution, $\boldsymbol{x}(\boldsymbol{q}_\alpha, a) = \boldsymbol{q}_\alpha + a\nabla_q \Phi_0(\boldsymbol{q}_\alpha)$, and $S(\boldsymbol{x}, a; \boldsymbol{q}) \geq S(\boldsymbol{x}, a; \boldsymbol{q}_\alpha)$ for $\boldsymbol{q} \not\equiv \boldsymbol{q}_\alpha$.

Solution (10) can be interpreted in terms of a simple geometrical construction. The paraboloid P is tangent to the random hypersurface Φ_0 at the point $\boldsymbol{q}_\alpha$. The Lagrangian point $\boldsymbol{q}_\alpha$ is where the particle came from, and the projection of the apex $\boldsymbol{x}$ is its Eulerian position. At early stages, the curvature of the paraboloid is greater than that of the hypersurface Φ_0, and there is a one-to-one correspondence between points in Lagrangian and Eulerian spaces when the Zel'dovich solution is valid. Later the pancakes form, which mean that some $\boldsymbol{x}$-points have two $\boldsymbol{q}$-originals. Intersection of pancakes forms the filaments, whose $\boldsymbol{x}$-points have three $\boldsymbol{q}$-originals in terms of solution (10), and intersection of filaments forms knots with four $\boldsymbol{q}$-originals (see Fig. 1 in Kofman et al. 1990).

Thus, in the adhesion model the problem of nonlinear gravitational evolution is reduced to geometrical analysis by inserting paraboloids into the random field of the initial linear gravitational potential φ_0. The artificial viscosity coefficient disappears from the answer (10) in the limit $\nu \to 0$, and time is involved in the result only as a parameter $a(t)$ determining the curvature of the paraboloid. The advantage of this model is that the skeleton of the LSS can be found at an arbitrary time with no consideration of previous evolution.

For now, our operating hypothesis is that the solution of the basic equations (1)–(3) can be approximately described by solution (10) of the adhesion model. The way to check this is to compare the matter distribution in numerical simulations of both cases.

Our numerical code for the adhesion model is based on the geometrical interpretation of the solution of the Burgers equation (eq. [10]); see Kofman et al. (1990) and Pogosyan (1989). The initial velocity potential Φ_0 and its derivatives are calculated on a square grid of size 512×512. The initial potential is a Gaussian random field consisting of the superposition of plane waves with random phases, under periodic boundary conditions. We have chosen initial fluctuations of density with power-law power spectra $P(k) \propto k^n$.

The aim of our two-dimensional code is the construction of the paraboloids simultaneously tangent to Φ_0 at two or three points at an arbitrary moment of time. The calculation consists of two steps. At the first step the grid points in the Lagrangian plane are sorted into two classes: (*a*) "free" particles which do not yet belong to any elements of structure (filaments or knots), and (*b*) "stuck" particles which by this time have stuck into the skeleton of the structure. The second step is correction of the position of the skeleton by mapping to Eulerian space (for details see Kofman et al. 1990).

Our numerical method of N-body simulation is a particle-mesh (PM) code of 512^2 particles on an equal mesh, with periodic boundary condition (for details see BDMPS). Both the adhesion and the N-body simulations use the same initial conditions. The N-body simulations have already been studied in many ways (Scherrer, Melott, & Shandarin 1991; Fry, Melott, & Shandarin 1992; Kauffmann & Melott 1992; Dominik & Shandarin 1992; BDMPS).

We use several different series to compare the results of N-body simulations with the adhesion model. We call them the Q series ($n = 2$), the J series ($n = 0$), and the N series ($n = -2$). These two-dimensional simulations are analogs of three-dimensional cases with $P(k) \propto k^{n-1}$. Thus the Q series are analogs of the three-dimensional pure Zel'dovich spectrum $P(k) = k$ [for the spectrum of the potential $\Delta(k) = k^{-3}$]. The N series are analogs (up to logarithmic correction) of the short-wave limit of the CDM spectrum. Each series Q, J, N is divided into three variants using a sharp cutoff of the power spectra at the harmonics $k = 4k_f$, $k = 32k_f$, and $k = 256k_f$, where k_f is the fundamental mode of the simulation square. Thus we have a set of series Q4, Q32, Q256; J4, J32, J256; and N4, N32, N256 respectively, which cover a very wide range of interesting possibilities. Additionally, we use the same realizations of phases for common harmonics in all of the simulations. The output time for each simulation has been chosen so as to compare them at the epoch when a specified mode $k_{\rm NL}$ enters the nonlinear regime,

$$\int_0^{k_{\rm NL}} d^2k\, P(k) a^2 = 1 .$$

In Figures 1–3 the moment when $k_{\rm NL} = 4k_f$ is chosen.

We compare the results of the N-body simulation and the adhesion model of the given series by displaying the particle positions and the skeleton of the structure for the same initial conditions and the same value of $k_{\rm NL}$ in the same figure. At the moment shown, the linearized density variance in all of the simulations with $k_c = 4$ is close to unity. Since in these cases the Zel'dovich approximation is known to be very good, it is not surprising that the adhesion model is also very good. Therefore we do not show them. All of Figures 1–3 correspond to the same $k_{\rm NL} = 4$, but the rms density fluctuations calculated from linear theory, $\sigma = (\langle \delta\rho/\rho \rangle^2)^{1/2}$ are very different and can be estimated from simple relations $\sigma_\rho = (256/k_{\rm NL})^2$, $(256/k_{\rm NL})$, and $[\ln(256/k_{\rm NL})]^{1/2}$ in the $n = 2$, $n = 0$, and $n = -2$ cases, respectively.

Obviously Figures 1 and 2 for the $n = -2$ and $n = 0$ simulations show very good visual agreement between the skeleton and the particle distribution in N-body simulations. Good agreement for these simulations was found for the all moments studied, not only for the chosen moments of Figures 1 and 2. However, at the stage most of the mass is in clumps and the discreteness of the system can be clearly seen in voids. This explains the absence of N-body counterparts for small branches of the skeleton. There is not such good agreement for the $n = 2$ simulation for the moment shown in Figure 3 when $k_{\rm NL} = 4$. We have checked the agreement for that series at other moments, and found good agreement between N-body simulations and the adhesion model of earlier moments of time. As an illustration, we plot in Figure 4 results of the $n = 2$ simulation, $k_c = 32$, at the moment when $k_{\rm NL} = 16$ and $\sigma \approx 4$ (which is obviously beyond the applicability of the Zel'dovich approximation).

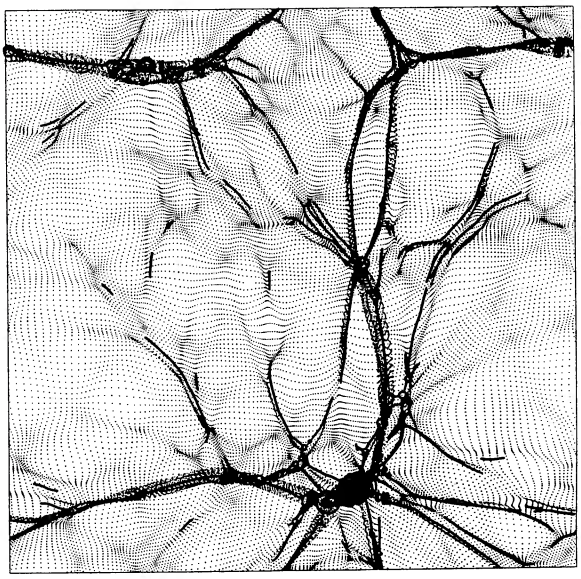

FIG. 1a

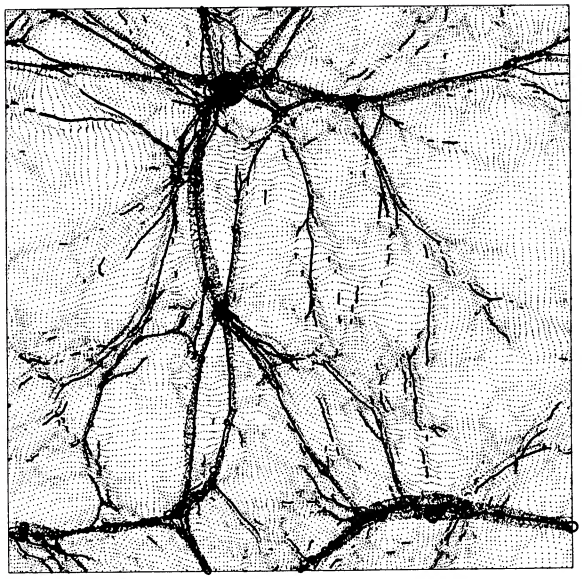

FIG. 1b

FIG. 1.—(*a*) Composite picture of the results of the *N*-body simulation and the adhesion model in the $n = -2$, $k_c = 32$ model. Dots show the distribution of particles in the *N*-body simulation. (Not all particles can be shown, but this is a fair sample.) Solid lines and circles represent the skeleton of the structure constructed in the adhesion model, with the same initial conditions, at the moment $\sigma = 1.65$. Solid lines show the positions of the paraboloid apices at double touching (filaments), and circles those at triple touching (knots). The radii of circles are proportional to the mass of knots. (*b*) Same as (*a*), but for $n = -2, k_c = 256$ series at the epoch $\sigma = 1.87$.

To find the reason why the adhesion model does not work so well beginning from some critical moment, as happens in the $n = 2$ simulation, we need to better understand structure formation. We will address the question in the next section. However, we would like to make one brief comment. At late times, when the skeleton of the structure is determined by the large-scale part of the potential φ, it can be represented by the sum of the initial potential φ_0 and an additional part $\delta\varphi$ due to nonlinear evolution. This extra part of the potential is generated by the local gravity of nonlinear clumps. If the typical scale of $\delta\varphi$ is smaller than the scale of significant correlation of the initial potential R_φ, then we expect that coherent initial motion is disturbed only a little by the local gravity. At still later times, the characteristic scale of the structure exceeds the scale R_φ, and local gravity dominates the motion. For the $n = 2$ simulation at the moment of Figure 3, the scale of the structure is larger than R_φ (Fig. 5; *filled hexagons*), and we do not expect the adhesion model to work accurately at this stage. This practically never happens in the $n = 0$ and $n = -2$ simulations, since the characteristic scale of the initial potential

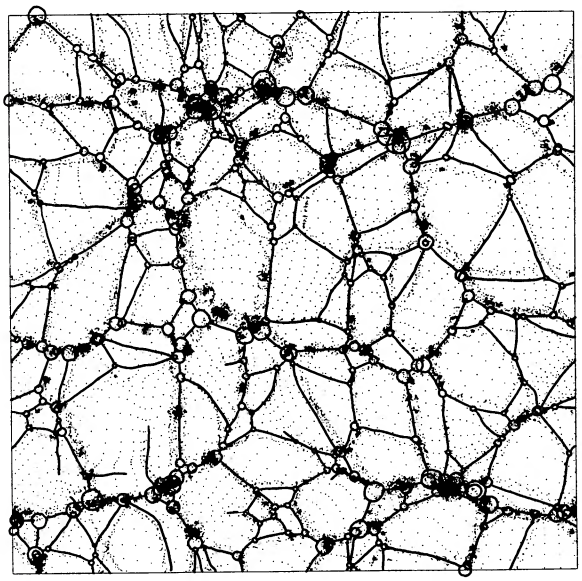

FIG. 2a

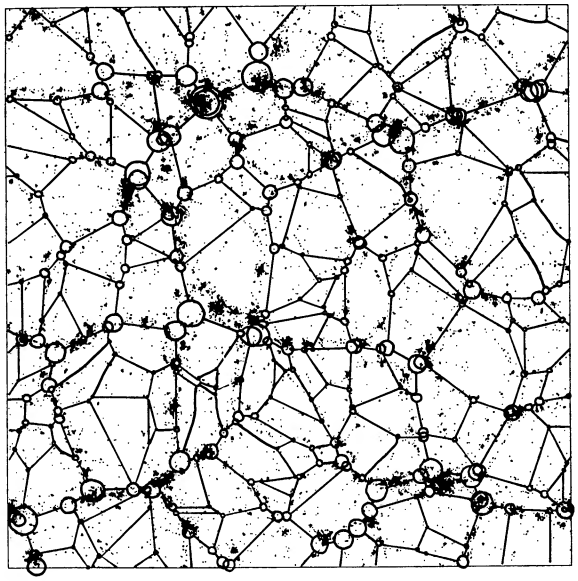

FIG. 2b

FIG. 2.—Same as Fig. 1, but for the following series and epochs, respectively: (*a*) $n = 0, k_c = 32, \sigma \approx 8$; (*b*) $n = 0, k_c = 256, \sigma \approx 64$

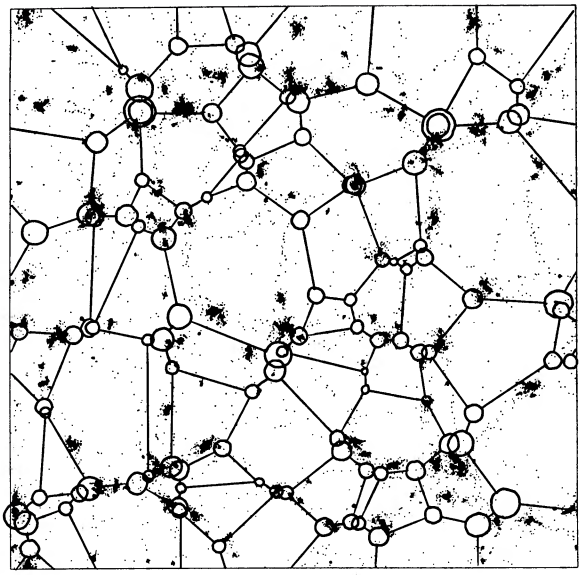

FIG. 3a

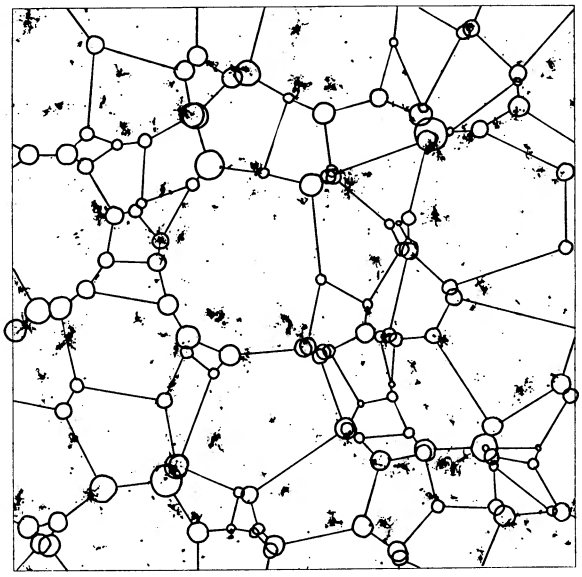

FIG. 3b

FIG. 3.—Same as Figs. 1 and 2, but for the following series and epochs, respectively: (*a*) $n = 2, k_c = 32, \sigma \approx 62.7$; (*b*) $n = 2, k_c = 256, \sigma \approx 4031$

roughly equals the size of the box (Fig. 5; two solid and dashed lines at the top). As a result, one observes good agreement between the adhesion model and the N-body simulations until the last stage, when very few clumps are left.

3. SUPERPANCAKES

One can easily see the prominent pancakes when the nonlinear stage begins in models with spectra having a sharp cutoff (Klypin & Shandarin 1983). In the CDM model (which has no sharp cutoff), the first N-body simulations (Melott et al. 1983) demonstrated the presence of highly connected, easily percolating structures, interpreted then as a filamentary distribution. Later simulations (e.g., Davis et al. 1985) confirmed the percolation result but did not emphasize the formation of pancakes or filaments. In later numerical simulations with higher mass resolution (Gelb & Bertschinger 1989; Park 1990) one can find coherent objects reminiscent of filaments. However, statements about the formation of the structural network in CDM–type models are strongly author-dependent. In two-dimensional high-resolution simulations one has enough particles to resolve the fine structures of matter distribution (Melott & Shandarin 1989). The more resolution, the more easily a prominent network structure is discovered, the interest in large-scale coherent structures has been "heated up" by observers, who noted the significant anisotropic structures already mentioned in § 1. By analogy, these also have become

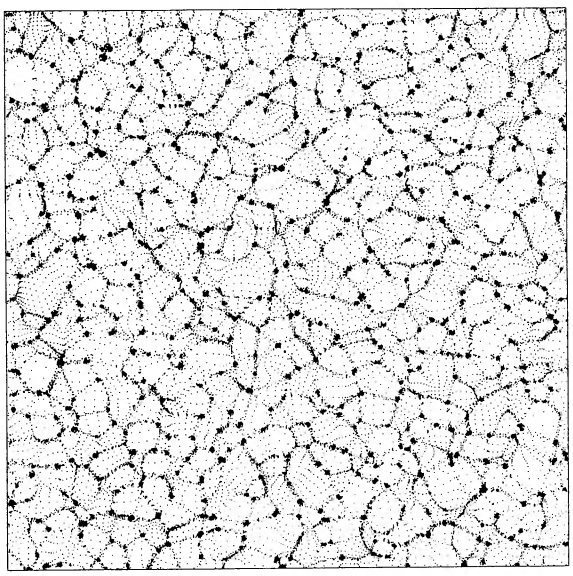

FIG. 4a

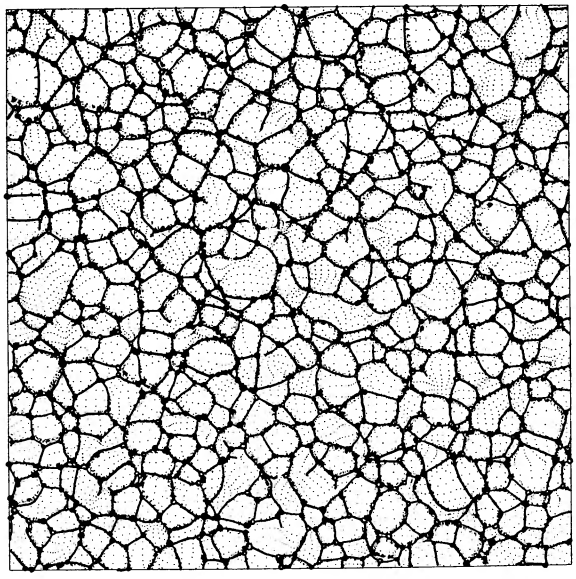

FIG. 4b

FIG. 4.—(*a*) Result of the N-body simulation in the $n = 2, k_c = 32$ series at the moment $\sigma = 4$. (*b*) Composite picture of the N-body simulation and the skeleton of the structure in the adhesion model in the $n = 2, k_c = 32$ series at the moment $\sigma \approx 4$. Same notation as in Figs. 1–3.

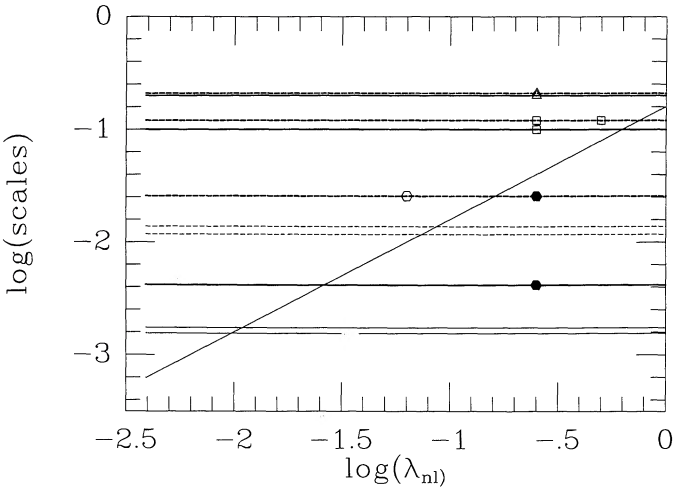

FIG. 5.—Relation of intrinsic scales to the scale of nonlinearity. The inclined line shows k_{NL}^{-1}. Horizontal lines show the scales of potential, velocity, and density fields for $k_c = 256$ (*solid lines*) and $k_c = 32$ (*dashed lines*). The three top lines in each series show $R_\varphi(n = -2)$, $R_\varphi(n = 0) = R_v(n = -2)$, and $R_\varphi(n = 2) = R_v(n = 0) = R_\rho(n = -2)$, respectively, from the top. The two bottom lines are $R_v(n = 2) = R_\rho(n = 0)$ and $R_\rho(n = 2)$, respectively, shown for comparison. Open triangles correspond to Figs. 1*a* and 1*b*; open squares to Figs. 2*a* and 2*b* and 6*a* and 6*b*; filled hexagons to Figs. 3*a* and 3*b*; and an open hexagon to Figs. 4*a* and 4*b*.

more prominent with more resolution (i.e., more complete surveys). We expect that in the future very larger surveys will make them of higher contrast relative to the background.

The adhesion model reveals what is behind large-scale coherent structures in simulations (and probably the universe as well), and provides a way to explain them. Let us recall, however, the hierarchical model based on the linear approximation. To linear order, density contrasts of the smoothed initial density field,

$$\frac{\delta\rho(\boldsymbol{x}, R)}{\rho} = \int d^3x' \, \frac{\delta\rho(\boldsymbol{x}')}{\rho} \, W(|\boldsymbol{x} - \boldsymbol{x}'|; R) , \qquad (13)$$

grow independently from perturbations on larger scales, for spectral index $n > -3$ in three dimensions or $n > -2$ in two dimensions. This result can be derived from timing arguments (Peebles 1980). If $v(r)$ is the initial (linear) velocity autocorrelation function, then $t(r) = r/v(r)$ roughly gives the epoch of the collapse of the objects of scale r. For power-law spectra $v(r) \propto r^{-(n+1)/2}$ and therefore $t(r) \propto r^{(3+n)/2}$, which says that for $n > -3$ (in three dimensions) $t(r)$ is a monotonically growing function. This line of argument implies that the motion of smaller clumps is uncorrelated on the scale of larger clumps, which form later mostly by means of two-clump merging. Obviously the greater the power on large scales, $n \to -3$ in three dimensions or $n \to -2$ in two dimensions, the less time between epochs of nonlinearity on small and large scales. In other words, the evolution proceeds faster as n decreases.

In our simulations the small-scale distributions in the $n = -2$ simulation (at the same k_{NL}) experience changes of two types when k_c increases from 4 to 256. The most dense regions become more clumpy, and the regions intermediate between high- and low-density regions become more filamentary. The whole distribution comes to look fractal. However, comparing the $k_c = 4$ (not shown), $k_c = 32$, and $k_c = 256$ cases, one can see that the large-scale structures are very similar, despite the fact that there is more power in the range $4 < k < 256$ than in the range $1 \leq k \leq 4$. Since computing power is finite, one can only speculate about distributions at $k_c \to \infty$. In particular, we believe that with increasing k_c the clumpiness of the structure will grow but the coherence of the large-scale structure will remain substantial. We believe that when fluctuations become quasi-linear the Zel'dovich approximation describes the distribution better than the direct extrapolation of the linear theory.

To a very restricted extent, one can think about this process as a superposition of pancakes of different scales, since in the $n = -2$ case all pancakes form nearly simultaneously. However, this interpretation has a very serious disadvantage. On the basis of such an interpretation one can argue that the superposition of random pancakes of various sizes produces an incoherent distribution. This argument is false because the Zel'dovich transformation of the initial perturbations to pancakes is *not* a linear procedure. Therefore, the linear combination of the initial perturbations at different scales does *not* produce a linear combination of random pancakes related to different parts of the initial spectrum.

In the more general case of arbitrary spectral index $n > -2$ (or $n > -3$ in three dimensions) the pancaking does not happen simultaneously on all scales. It is possible that on small scales one has an overdeveloped cellular structure and that on large scales the degree of nonlinearity corresponds to the first large-scale pancakes. These large-scale pancakes are constructed *not only* from free particles which were not stuck in the structure before, but also from elements of cellular structure (knots and filaments) which formed earlier.

For illustration let us follow the further time evolution of LSS in the $n = 0$, $k_c = 32$ simulation. In Figure 6*a* it is shown at the moment when $k_{NL} = 2$ or $\sigma_\rho = 16$. The skeleton of the adhesion model coincides closely with the particle positions from the N-body simulation. It is easy to recognize high-contrast coherent structures in addition to the network of filaments, many of them remaining from the stretched pancakes of the first generation. The structure we refer to consists of alignment of clumps of particles, and it can be explained as a result of the coherent motion not only of free particles but also of knots of cellular structure, on which large-scale coherent motion is impressed.

A visual check of these ideas provides strong support. The reader is urged to examine the process of evolution particularly in all of the $k_c = 256$ series, whose time dependence is shown in the accompanying videotape, Segment 1. One can see here the coherent motion of the knots to form superpancakes, as well as the disruption of this process in the $n = 2$ case.

As a further check of the assumption about successive pancaking over various scales at various times (as a model of escalating nonlinearity), let us not filter the initial fluctuations of the gravitational potential on scale R,

$$\varphi(\boldsymbol{x}, R) = \int d^3x' \varphi(\boldsymbol{x}) W(|\boldsymbol{x} - \boldsymbol{x}'|; R) . \qquad (14)$$

Our filter is a step function in k-space: $W(k) = \theta(k - k_R)$; $k_R = 4$. The skeleton in the adhesion model after such filtering is shown in Figure 6*b* (for the $n = 0$, $k_c = 32$ simulation). We see good agreement between filaments in the adhesion model with smoothing and the largest coherent structures in the N-body simulation with no smoothing. We call the large-scale, anisotropic, coherent structures, formed as a result of long wave perturbations which just have entered the nonlinear regime, "superpancakes" and "superfilaments," in order to distinguish

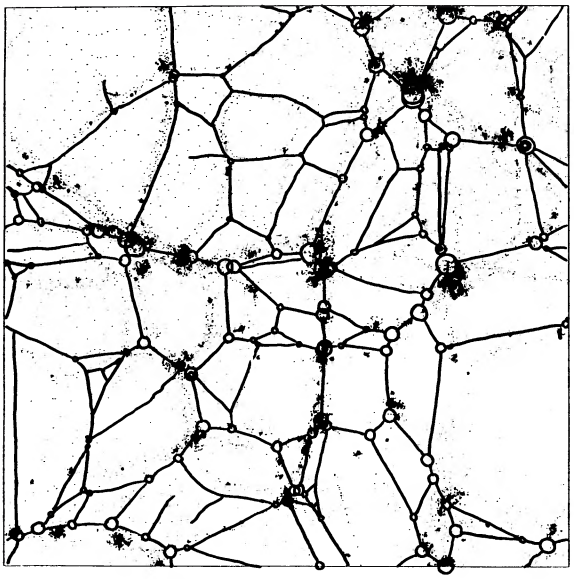

FIG. 6a

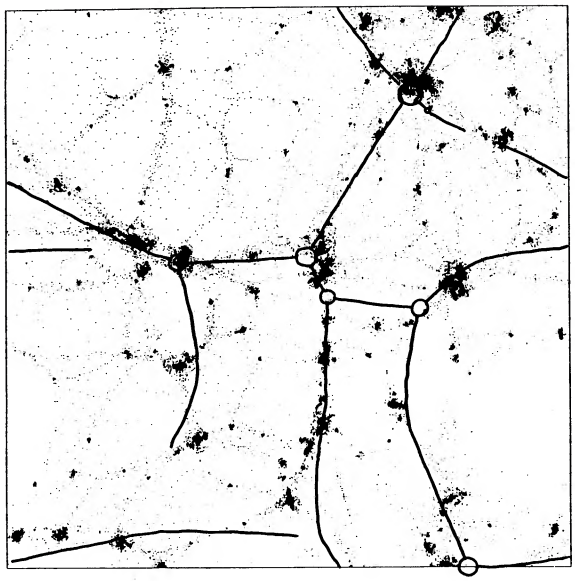

FIG. 6b

FIG. 6.—(*a*) Same as Figs. 1–3, but for the series $n = 0, k_c = 32$ at the moment $k_{NL} = 2$, $\sigma \approx 16$. (*b*) Composite picture of the result of the *N*-body simulation in the $n = 0, k_c = 32$ series at the moment $\sigma \approx 16$, and the skeleton of the adhesion model at the same moment but with paraboloids inserted in the initial potential, filtered up to the four lowest harmonics and with the same phases as in (*a*).

them from those which arise on smaller scales in the first generation. We conclude that these structures are not visual artifacts but results of coherent motion on corresponding scales. (Additional experimental support for these ideas can be found in the cross-correlation studies presented in BDMPS.)

As in hierarchical clustering, the successive pancaking on larger scales washes out smaller structures to some extent. At the given moment t, when the typical size of the structure is $l(t)$ (which is close to k_{NL}^{-1}), the initial potential on small scales $k^{-1} \ll k_{NL}^{-1}$ is almost irrelevant. In particular, it means that two series with differences only on small scales (say, one of them has a sharp cutoff on $k > k_0$) have nearly the same evolution at late times $[t \gg t(k_0)]$. More specifically, it means that the largest structures are similar but the smallest ones can be different (compare Figs. 2*a* and 2*b* or Figs. 6*a* and 6*b*). Gurbatov & Saichev (1981) pointed out that in the case of one-dimensional Burgers turbulence, large-scale structures at late times depend only on the large-scale asymptote of initial fluctuations. In this connection, let us comment on the results of Weinberg & Gunn (1989, 1990), where a different numerical technique to solve the Burgers equation (9) was used, based on the convolution integral in the analytical solution with finite viscosity. This actually corresponds to an effective smoothing of initial fluctuations. The agreement shown there between the large-scale matter distribution in *N*-body simulations of the CDM model and that in the adhesion model with an effective smoothing just means that the same-scale details of structure are dynamically forgotten and unimportant at large scales on late stages (see also Little Weinberg, & Park 1991). Another result which corresponds to effective similarity between nonlinear clustering and smoothing is the reduction in amplitude of the topological genus with dynamical evolution in hierarchical clustering models found by Melott, Weinberg, & Gott (1988).

We believe that the major feature of superpancaking—the coherent motion of mass clumps—can be traced using the adhesion model until the scale of nonlinearity k_{NL}^{-1} reaches the characteristic scale of the initial potential R_φ. The escalation of superpancaking also finishes on the maximal scale R_φ. This scale is the length of significant correlation of the random field of φ_0. For a Gaussian field R_φ can be defined from the expansion of the correlation function $\xi_\varphi(r) = \xi_\varphi(0)(1 - r^2/2R_\varphi^2 + \cdots)$:

$$R_\varphi = (2D)^{1/2} \frac{\sigma_0}{\sigma_1}, \tag{15}$$

where D is the dimension and σ_0 and σ_1 are dispersions of the potential and its gradient, respectively. Since we deal with finite ranges in this work, R_φ exists in all our models. There are of course cases when R_φ formally does not exist. In such cases one has to use a more sophisticated approach and use a different characteristic of φ, such as the structure function, for example. We do not discuss it here. After the characteristic scale of nonlinearity k_{NL}^{-1} exceeds R_φ, then most of the filaments predicted by the adhesion model correspond to one or two clumps (Figs. 3*a* and 3*b*). This, of course, means that one cannot talk about filamentary structure at all. The evolution becomes "pure" hierarchical clustering. For instance, the Q $(n = 2)$ series with $k_c = 256$ lives in this limit most of the time. Figure 5 demonstrates the evolution of structure in terms of k_{NL}^{-1} against R_φ calculated according to equation (15) for all our series.

The relation between the hierarchical clustering theory (and the closely related Press-Schechter formalism) and continuous pancaking can be seen in terms of the distribution of eigenvalues of the deformation tensor of the smoothed field. According to the pancake model, the superpancakes will form approximately in the Lagrangian regions where the largest of the eigenvalues λ_1 of the smoothed field has a maximum (Zel'dovich 1970). On the other hand, the hierarchical clustering theory predicts the formation of mass concentrations in regions where $\delta\rho/\rho$ is proportional to $(\lambda_1 + \lambda_2 + \lambda_3)$, so both predictions should correlate to some extent. According to Shandarin & Klypin (1984), a somewhat more accurate prediction of the positions of the clumps can be made by relating them to the positions of maxima of the third eigenvalue λ_3 (the second in 2D).

4. STATISTICAL PROPERTIES OF STRUCTURE

The skeleton of the matter distribution found in the adhesion model corresponds reasonably well to the structure from N-body simulations until the epoch t_φ when $k_{\rm NL}^{-1} \approx R_\varphi$. Let us recall that in two dimensions a filament in the Eulerian space is a set of the projections of the apices of paraboloids, each of which has two points of contact with the φ_0-surface in Lagrangian space. A knot in the projection of a paraboloid which has three points of contact. At quite late times, a Lagrangian region which has been included in a knot evolves to a triangle (asymptotic shape), whose vertices are these three points of contact. Then the whole Lagrangian space is divided into triangles, corresponding to knots of the cellular structure. The remaining gaps between triangles in Lagrangian space correspond to the Lagrangian images of filaments which connect knots. At late times there is a very small fraction of free particles (not stuck into structure).

Thus one can operate with well-defined values: the area S of triangles, corresponding to knots of the mass, is $m = \bar{\rho}S$; the area of cells is A; and the comoving velocity of knots is $\boldsymbol{U}$. The velocity of a knot is determined by a geometrical condition (Gurbatov et al. 1989; Kofman et al. 1990) and can be found by solving the following system of algebraic equations:

$$\begin{aligned} \boldsymbol{U} \cdot (\boldsymbol{q}_1 - \boldsymbol{q}_2) &= \Phi_0(\boldsymbol{q}_2) - \Phi_0(\boldsymbol{q}_1) , \\ \boldsymbol{U} \cdot (\boldsymbol{q}_1 - \boldsymbol{q}_3) &= \Phi_0(\boldsymbol{q}_3) - \Phi_0(\boldsymbol{q}_1) , \end{aligned} \tag{16}$$

where $\boldsymbol{q}_1, \boldsymbol{q}_2, \boldsymbol{q}_3$ are the three points of contact. It is easy to see that from the geometrical point of view the velocity of knot is a vector in a three-dimensional space $(\Phi_0, \boldsymbol{q})$, with direction normal to the triangle constructed on the points of contact with the Φ_0-surface in this space and magnitude proportional to its area.

Let us illustrate how triangulation of the Lagrangian space corresponds to the Lagrangian regions of clusters obtained from N-body simulation. We picked the three most massive clusters from the $n = 0$, $k_c = 32$ simulation at the late moment $k_{\rm NL} = 2$ or $\sigma_\rho = 16$ (see Fig. 6). The corresponding Lagrangian regions are shown in Figure 7. In Figure 7*a* we also plot the triangles of knots from the adhesion model corresponding to these clusters. In Figure 7*b* we show for comparison the same Lagrangian regions of the largest clumps together with initial density contours after filtering on the scale corresponding to the mass of the selected clumps. It turns out that clusters from N-body simulations correspond not to one knot but rather to *several knots* of an auxiliary skeleton structure, contrary to the simple assumption of previous papers on the adhesion model.[2] Physically this is connected with the fact that the adhesion model is based on the Zel'dovich approximation, which does not take into account purely local gravitational forces and which therefore does not describe the merging of clusters accurately enough. Also, pointlike knots merge later than the clumps of finite size. One can get a rough idea about the advantages and disadvantages of both approximations by comparing Figures 7*a* and 7*b*.

We therefore must develop some technique to model the clustering of knots. One way is to do the triangulation of the Lagrangian space using a smoothed potential field. In this procedure a large triangle of the smoothed field plays only a role of indicator for combining original triangles constructed in the unsmoothed field into a clump. We leave this question for another paper, but for now we note that there is a way to cluster knots to get a mass multiplicity function which is in good agreement with that from N-body simulations.

In early papers on the statistics of the solution of the one-

[2] Scherrer & Melott (1987) encountered the same problem when they found that there was not a one-to-one correspondence between cosmic string loops and collapsed objects, so that cluster-cluster correlations in the cosmic string model did not obey the expectations of earlier, simple, analytic calculations.

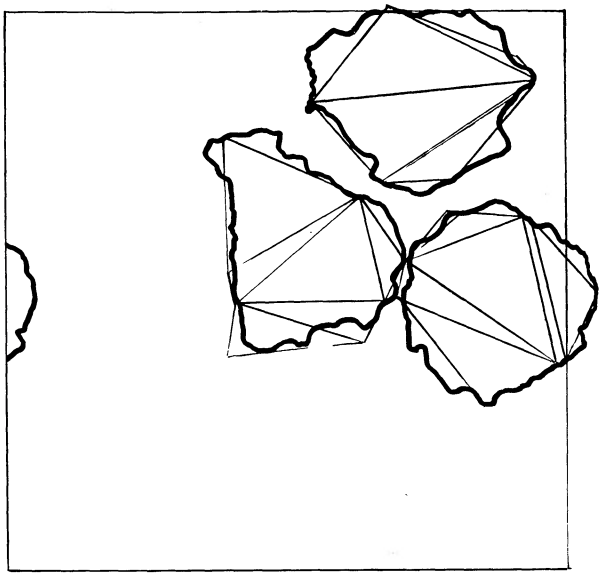

FIG. 7*a*

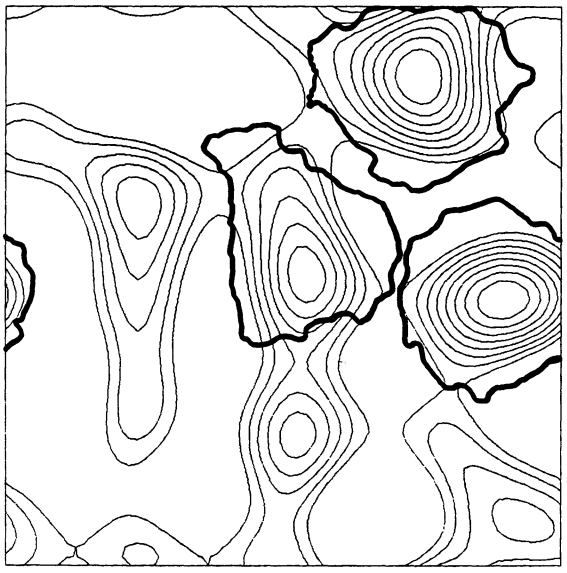

FIG. 7*b*

FIG. 7.—(*a*) Bold lines show the borders of the Lagrangian regions of the three most massive clusters from the N-body simulation in Fig. 6 for $n = 0$, $k_c = 32$, $\sigma \approx 16$. Solid-line triangles correspond to the Lagrangian regions of knots of the skeleton in Fig. 6*a*, which are adjusted to these clusters. (*b*) Bold lines as in (*a*). Solid lines show the contours of the initial density field of the N-body simulation of the $n = 0$, $k_c = 32$ series in Fig. 6, filtered up to the four lowest harmonics. This filtering scale approximately corresponds to the masses of clusters of (*a*).

dimensional Burgers equation (outside the cosmological context; Kida 1979; Gurbatov & Saichev 1981) and on the adhesion model in cosmology (Gurbatov, Saichev & Shandarin 1989; Doroshkevich & Kotok 1990), analytical calculations have been made under the following assumptions: (1) a single knot is associated with a single matter clump and (2) at the latest times only high peaks of the initial potential are important, and they are assumed to be uncorrelated.

The main result of these calculations is the self-similarity of the velocity and mass distribution functions of knots. The distribution function of sizes of cells was found only in the one-dimensional case under these conditions (Kida 1979).

As we have seen, the first assumption is not very good for two-dimensional systems, except probably for knots of very small mass. We believe that this is *also true* in three dimensions, and we will test it soon.

The second assumption corresponds to the stages of evolution ($k_{\rm NL}^{-1} > R_\varphi$) when we expect that neither the two- nor the three-dimensional adhesion models predicts the skeleton of the matter distribution very accurately (see, e.g., Figs. 3*a* and 3*b*). Here we consider the distribution functions of velocities and masses of knots and areas of cells from our two-dimensional numerical calculations of the skeleton of structure in the adhesion model. We focus on checking the scaling properties of the structure, as a test for the adhesion model.

For statistical study we use the series $n = 0$ and $n = 2$ (both with $k_c = 256$) at early times because the larger numbers of cells provide better statistics. In Figures 8*a* and 8*b* we plot the mass multiplicity function for bare knots of the skeleton obtained in the adhesion model, for both series and for different moments of time corresponding to $k_{\rm NL} = 32$, 16, and 18. We can see the self-similar evolution of this function, using mass scaling in units of the characteristic mass M_*, as is usually done for the multiplicity function (see, for example, Efstathiou et al. 1988). We find $M_* \propto a^2$ for the $n = 0$ series and $M_* \propto a$ for the $n = 2$ series, in agreement with the scaling laws derived from the simple linear theory.

In Figure 9 we present the distribution $F(|U|)$ of the velocities of knots U. The time evolution of the velocity distribution function of knots is remarkably self-similar. The characteristic velocity scales are $U_* \sim (\ln k_{\rm NL})^{1/2}$ for the $n = 0$ series ($k_{\rm NL} \sim a^{-1}$), and $U_* \sim k_{\rm NL}$ for the $n = 2$ series ($k_{\rm NL} \sim a^{-1/2}$), which are also consistent with the linear theory. In addition, the distribution function of the velocity components is fitted well by the Gaussian law. The Gaussian character of the knots' velocity distribution function was found analytically by Gurbatov et al. (1989), but under the assumption of uncorrelated peaks at late times. The present result was obtained without that assumption and suggests that it can be more general.

In Figure 10 we show the distribution function of areas of cells A (the two dimensional analog of volumes of voids). We find the self-similarity of the distribution function with respect to A/A_*, where A_* is a characteristic area. We find $A_* \propto a^\alpha$, where $\alpha \approx 1$ for the $n = 2$ series and $\alpha \approx 1.6$ for the $n = 0$ series. The former is in agreement with the assumption that $M_* \propto A_*$, but the latter is not. Taking into account that the scaling was checked only for three values of $k_{\rm NL}$, one can easily interpret that as an indication of change in slope from $A_* \propto a^2$ related to the finite size of the box. This departure from the slope expected in the linear theory has been studied more thoroughly by Kauffmann & Melott (1992). Both results are in qualitative agreement despite the different definitions of voids. The tail of the distribution at large A is fitted well by an exponential law

$$N(A) \propto \exp(-A/A_*) . \tag{17}$$

A similar asymptote in the one-dimensional case was found by Kida, but again under the assumption of uncorrelated peaks. The fact that a matter clump corresponds to a few knots of cellular structure leads to the conclusion that some cells of small areas are artificial and are not associated with voids in the matter distribution. However, we expect a good correspondence between large cells in the adhesion model and voids in

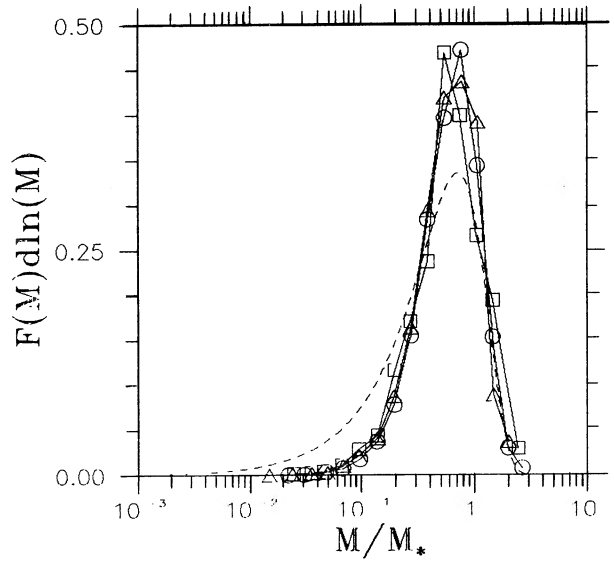

FIG. 8*a*

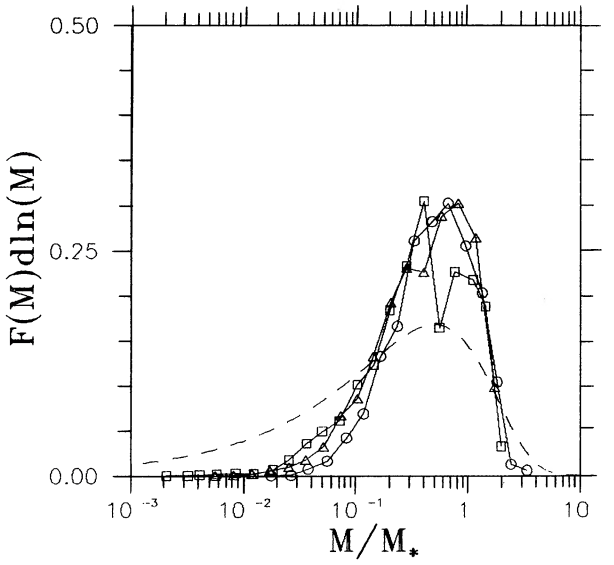

FIG. 8*b*

FIG. 8.—(*a*) Mass-of-knots multiplicity function $F(M)$ in the adhesion model in the Q256 ($n = 2$, $k_c = 256$) series for moments $k_{\rm NL} = 32$, $\sigma \approx 64$ (*circles*), 16, 256 (*triangles*) and 8, 1024 (*squares*). Mass is given in units of characteristic mass M_*. The dashed line corresponds to the Press-Schechter formula. (*b*) Same as (*a*), but for the J256 ($n = 0$, $k_c = 256$) series for moments $k_{\rm NL} = 32$, $\sigma \approx 8$ (*circles*), 16, 16 (*triangles*) and 8, 32 (*squares*).

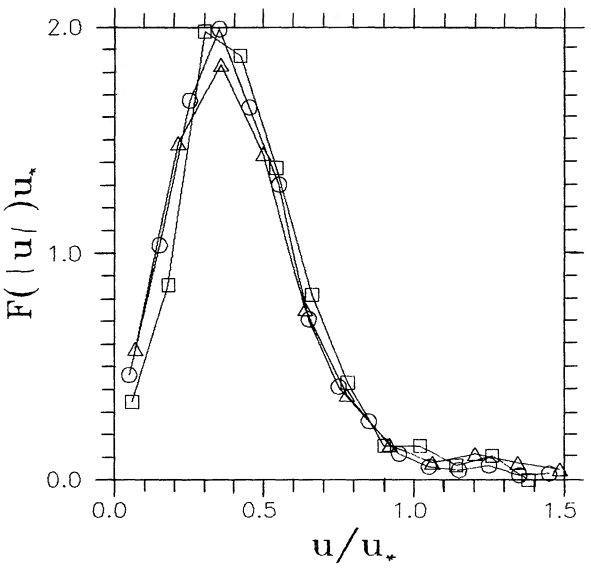

FIG. 9a

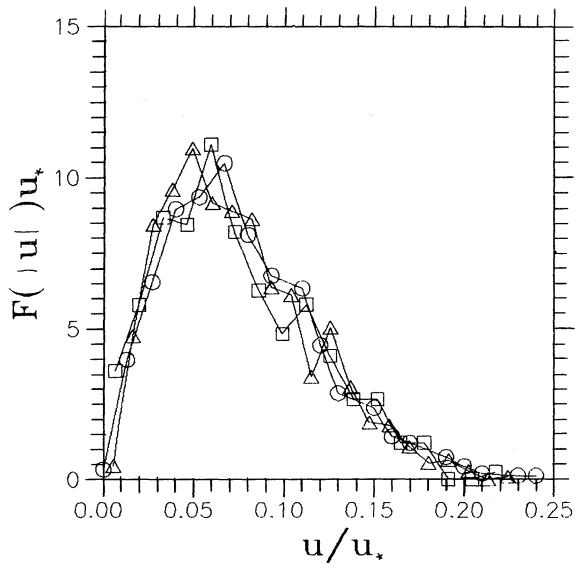

FIG. 9b

FIG. 9.—(*a*) Velocity-of-knots U distribution function $F(|U|)$ in the adhesion model for $n = 2$, $k_c = 256$; same moments of time. Velocity is given in units of the characteristic scale U_*. (*b*) Same as (*a*) but for the series $n = 0, k_c = 256$.

N-body simulations, including the cases following the law in equation (17). Kauffmann & Melott (1992) show the self-similarity of cell areas A in N-body simulations and discuss under what conditions this may break down because of the finite size of the simulations. They find that N-body methods work best in models like $n = 2$, where adhesion fails earlier. Thus, the two approaches are complementary. Adhesion works best in those cases where N-body methods have the greatest difficulty, and it offers a tool for analytical estimation. In the next natural step, we will compare statistics of voids in both methods, in two and three dimensions.

5. DISCUSSION

We tested the adhesion model against two-dimensionsal N-body simulations of power-law models $P(k) \propto k^n$, ($n = +2$, 0, -2) with three different cutoffs, $k_c = 256k_f$ (Nyquist frequency), $32k_f$, and $4k_f$, with k_f corresponding to the fundamental mode. Our results confirm previous tests of the adhesion model (Kofman et al. 1990; Weinberg & Gunn 1989, 1990; Nusser & Dekel 1990) and demonstrate good agreement between the matter distribution in N-body simulations and the skeleton from the adhesion model for a wide range of initial conditions. The new results are as follows.

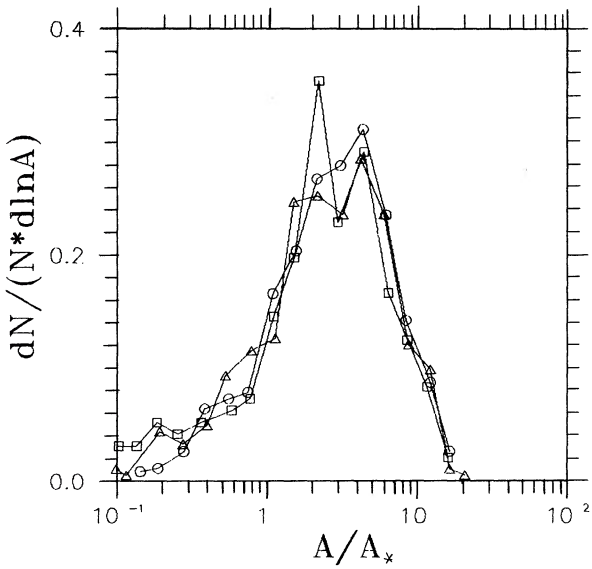

FIG. 10a

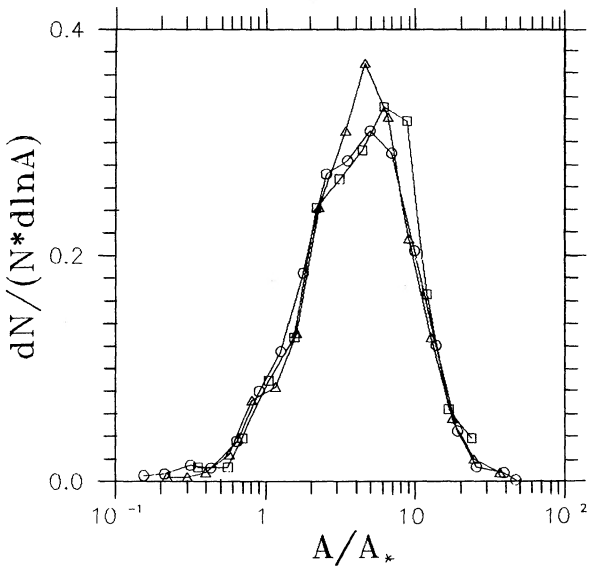

FIG. 10b

FIG. 10.—(*a*) Area-of-cells distribution function $N(A)$ in the adhesion model for the Q256 series for the same moments. The area is given in the units of characteristic area A_* (*b*) Same as (*a*), but for the J256 series at the same moments.

The restrictions on the model can be formulated in terms of the characteristic scale R_φ of the initial gravitational potential, corresponding to the length of substantial positive correlation. The adhesion model demonstrates good agreement with N-body simulations until the scale of nonlinearity reaches R_φ (see Figs. 1, 2, 4, and 6, and see Fig. 5 [*open symbols*]). At later stages it loses good one-to-one correspondence (see Figs. 3*a* and 3*b* and Fig. 5 [*filled symbols*]), though it may be correct in a statistical sense, similar to the Press-Schecter model (Williams et al. 1991; Bond et al. 1990). We can suggest the following explanation for this limitation. Nonlinear gravitational instability can be described as the motion of clumps and their merging into larger clumps. The motion can be roughly divided into two components, one corresponding to the initial velocity perturbation and the other generated locally by nearby nonlinear clumps. The adhesion model describes the motion due to initial velocity perturbations very well, but the local part is described much more poorly. The immediate result of this is that the process of merging may be incorrect in the adhesion model. While the scale of nonlinearity is small compared to R_φ, the initial component of the velocities of the clumps is large enough and the adhesion model works well. At later stages, a substantial part of clump velocities is determined by local gravity, which is poorly represented in the adhesion model, explaining the disagreement.

The component of motion of clumps related to the initial velocity field causes the pancaking of clumps on scales smaller than R_φ (for illustration see the accompanying videotape, Segment 1). This interpretation is actually similar to the idea of applying an ensemble of filtered linear density fields to the hierarchical clustering model, except that we suggest taking the ensemble of the filtered linear potential fields and applying the Zel'dovich approximation to describe the evolution of the filtered field. As a result, the coherent motion of the clumps produces structures similar to pancakes or filaments. However, they are not as sharp as the caustics corresponding to the first-generation pancakes. Instead, they are clumpy, and because of that we call them superpancakes or superfilaments. Their typical scale increases with time until it reaches the biggest superpancake scale, which is about R_φ. Smoothed with the appropriate scale, one can see non-Gaussian distribution of density contours, though the amplitude $\delta\rho/\rho$ is less than unity. Applying these results to cosmology, we get in the standard CDM model $R_\varphi \approx 6^{1/2}(\sigma_0/\sigma_1) \approx 50\ h^{-1}$ Mpc, where $h \equiv H/100$ km s^{-1} Mpc^{-1} as usual, and a long-wave cutoff at the horizon scale was applied. According to our criterion $R_\varphi > k_{\rm NL}^{-1} \approx 5\ h^{-1}$ Mpc, the adhesion model could be applied to the CDM cosmological model until the present epoch, which is in good agreement with the results of Weinberg & Gunn (1989, 1990).

We have compared the Lagrangian regions of clusters in N-body simulations with those in the adhesion model. It turns out that the largest clumps of matter generally are associated with several knots of cellular structure. One has to use an additional procedure of clustering of knots in the adhesion model.

In the previous papers on the adhesion model, analytical calculations were done based on oversimplified assumptions of uncorrelated high peaks of gravitational potential at late times, and one-to-one correspondence between clumps and knots of skeleton. The result of those calculations was a self-similarity of evolution of structure. In this paper we found that both assumptions are inapplicable to gravitational systems. The adhesion model also works in the opposite case of correlated peaks of gravitational potential sitting on the same slope of the initial potential hypersurface. In numerical simulations of the adhesion model, we studied the scaling properties of the evolution of the distribution function for the masses of knots, and we found the mass function $F(M)$, the distribution function of velocities of knots $F(|U|)$, and the distribution function of areas of cells $N(A)$ for the $n = 2$ spectrum. A challenge is to calculate these functions analytically in the adhesion model. In addition, we found that the velocity distribution function closely fits a Gaussian law. The tail of the distribution function of the areas of cells (voids) is exponential.

We thank Jim Peebles for many useful conversations related to the subject of the paper. In particular, we are very grateful to David Weinberg for discussion and many useful comments. Our clustering simulations were performed at the National Center for Supercomputing Applications (Urbana, IL). We are grateful for financial support from NASA grants NAGW-1288, and NAGW-2455, and from NSF under grant AST-9021414. L. K. gratefully acknowledges a grant for the CIAR Cosmology program. A. L. M. wishes to acknowledge University of Kansas GRF grant 3521-20-0038.

REFERENCES

Bardeen, J. M., Bond, J. R., Kaiser, N., & Szalay, A. S. 1986, ApJ, 304, 15
Beacom, J. F., Dominik, K. G., Melott, A. L., Perkins, S., & Shandarin, S. F. 1991, ApJ, 372, 351 (BDMPS)
Bond, J. R., Cole, S., Efstathiou, G., & Kaiser, N. 1991, ApJ, 379, 440
Burgers, J. M. 1974, The Nonlinear Diffusion Equation (Dordrecht: Reidel)
Chincarini, A., Rood, H., & Thompson, L. 1981, ApJ, 249, L47
Davis, M. G., Efstathiou, G., Frenk, C., & White, S. D. M. 1985, ApJ, 292, 371
Dekel, A. 1983, ApJ, 264, 373
Dominik, K., & Shandarin, S. F. 1992, ApJ, 393, 450
Doroshkevich, A. G., & Kotok, E. V. 1990, MNRAS, 246, 10
Doroshkevich, A. G., Kotok, E. V., Novikov, I. D., Polyudov, A. N., Shandarin, S. F., & Sigov, Yu. S. 1980, MNRAS, 192, 321
Efstathiou, G., Frenk, C., White, S. D. M., & Davis, M. 1988, MNRAS, 235, 715
Fry, J. N., Melott, A. L., & Shandarin, S. F. 1992, ApJ, 393, 431
Gelb, J., & Bertschinger, E. 1989, BAAS, 21, 1172
Geller, M., & Huchra, J. 1989, Science, 246, 897
Giovanelli, R., & Haynes, M. 1982, AJ, 87, 1355
Gott, J. R., Mellot, A. L., & Dickinson, M. 1986, ApJ, 306, 41
Gurbatov, S. N., & Saichev, A. I. 1981, Soviet Phys.—JEPT, 80, 689
Gurbatov, S. N., Saichev, A. I., & Shandarin, S. F. 1985, Soviet Phys. Dokl. 30, 921
———. 1989, MNRAS, 236, 385
Kaiser, N. 1984, ApJ, 284, L9
Kauffmann, G., & Melott, A. L. 1992, ApJ, 393, 415
Kida, S. 1979, Fluid Mech., 93, 337
Klypin, A. A., & Shandarin, S. F. 1983, MNRAS, 204, 891
Kofman, L. A. 1991, in Proc. IUAP Conference on Nucleosynthesis in the Universe, ed. K. Sato (Dordrecht: Kluwer)
Kofman, L. A., Pogosyan, D. Yu., & Shandarin, S. F. 1990, MNRAS, 242, 200
Kofman, L. A., & Shandarin, S. F. 1988, Nature, 334, 129
Little, B., Weinberg, D., & Park, C. 1991, MNRAS, 253, 307
Melott, A. L. 1983, MNRAS, 204, 7
Melott, A. L., Einasto, J., Saar, E., Suisalu, I., Klypin, A. A., & Shandarin, S. F. 1983, Phys. Rev. Lett., 51, 935
Melott, A. L., & Shandarin, S. F. 1989, ApJ, 343, 26
———. 1990, Nature, 346, 633
Melott, A. L., Weinberg, D. H., & Gott, J. R. 1988, ApJ, 328, 50
Nusser, A., & Dekel, A. 1990, ApJ, 362, 14
Oort, J. 1983, ARA&A, 21, 373
Park, C. 1990, MNRAS, 242, 59P
Peacock, J., & Heavens, A. 1990, MNRAS, 243, 133
Peebles, 1980, P. J. E. 1980, The Large-Scale Structure of the Universe (Princeton: Princeton Univ. Press)
Pogosyan, D. Yu. 1989, Tartu preprint (Estonian Acad. Sci.)
Press, W. H., & Schechter, P. 1974, ApJ, 187, 425
Scherrer, R. J., & Melott, A. L. 1987, Nature, 328, 691
Scherrer, R. J., Melott, A. L., & Shandarin, S. F. 1991, ApJ, 377, 29

Shandarin, S. F. 1988, in Large Scale Structure in the Universe, ed. J. Audouze, M. Ch. Peleton, & A. Szalay (Dordrecht: Kluwer), 273
Shandarin, S. F., Doroshkevich, A. G., & Zel'dovich, Ya. B. 1983, Soviet Phys.—Uspekhi, 26, 46
Shandarin, S. F., & Klypin A. A. 1984, Soviet Astron., 28, 491
Shandarin, S. F., & Zel'dovich, Ya. B. 1989, Rev. Mod. Phys., 61, 185
Tago, E., Einasto, J., & Saar, E. 1986, MNRAS, 206, 177
Weinberg, D., & Gunn, J. 1989, ApJ, 352, L25
———. 1990, MNRAS, 247, 260
Williams, B. G., Heavens, A. F., Peacock, J. A., & Shandarin, S. F. 1991, MNRAS, 250, 458
Zel'dovich, Ya. B. 1970, A&A, 5, 84
Zel'dovich, Ya. B., & Novikov, I. D. 1983, The Structure and Evolution of the Universe (Chicago/London: Univ. Chicago Press).